

## Diffuse-magnetic-scattering calculations for frustrated antiferromagnets

Jan N. Reimers

*Department of Physics, Simon Fraser University, Burnaby, British Columbia, Canada V5A 1S6*

(Received 21 October 1991)

A method based on the Gaussian approximation is presented for calculating the magnetic neutron scattering from short-range-ordered magnetic systems. Scattering profiles are calculated for three highly frustrated systems: the rhombohedral-, *kagomé*-, and pyrochlore-lattice antiferromagnets. The results are compared with those obtained from conventional Monte Carlo techniques and with recent experimental results for  $\text{FeF}_3$  and  $\text{Tb}_2\text{Mo}_2\text{O}_7$ . For the rhombohedral lattice, the calculations predict two-dimensional peaks even in the presence of strong interplanar interactions and provide an explanation for the lack of observed wide-angle magnetic neutron scattering in  $\text{LiNiO}_2$ . Scattering consistent with short-range order is predicted for the pyrochlore- and *kagomé*-lattice antiferromagnets down to very low temperatures. The Monte Carlo method is most successful for treating truly short-range-ordered systems and low-dimensional systems. The Gaussian approximation method gave similar results for these systems and was also found to be useful for three-dimensional systems with quasi-low-dimensional order where the Monte Carlo method was impractical.

### I. INTRODUCTION

Geometrically frustrated antiferromagnets exhibit unusual and interesting properties such as large ground-state degeneracies,<sup>1,2</sup> incommensurate and noncoplanar long-range order,<sup>3</sup> novel critical properties,<sup>4</sup> and spin-glass behavior.<sup>5</sup> A firm understanding of periodic frustrated antiferromagnets is also believed to be a prerequisite for understanding the spin-glass problem.

The two-dimensional triangular lattice antiferromagnet is the best known geometrically frustrated system. The Ising case was solved by Wannier.<sup>1</sup> It exhibits no long-range order at any temperature and has a macroscopic ground-state degeneracy, and therefore a large zero-point entropy  $S(T=0) \propto N$ , where  $N$  is the number of spins. For vector spins a noncollinear three sublattice  $120^\circ$  spin arrangement forms. The simplest three-dimensional stacking of the triangular sheets ( $\cdots AAA \cdots$ ) with a corresponding interplanar ferromagnetic or antiferromagnetic interaction, does not have a profound effect on the nature of the in-plane magnetic order. However, the rhombohedral stacking [ $\cdots ABCABC \cdots$ , see Fig. 1(a)] in which successive planes are offset so as to form a cubic close-packed array, leads to much more complex behavior. In the rhombohedral stacking, interplanar interactions of either sign will result in additional magnetic frustration over and above the in-plane frustration. The interplane interactions prefer collinear spin arrangements, while the in-plane interactions are best satisfied by the noncollinear  $120^\circ$  structure.

To proceed with calculations concerning the rhombohedral-lattice antiferromagnet, we use a Heisenberg Hamiltonian written in terms of Fourier modes

$$\mathcal{H} = -\frac{1}{2} \sum_{\mathbf{q}} J_{\mathbf{q}} \mathbf{S}_{\mathbf{q}} \cdot \mathbf{S}_{-\mathbf{q}}, \quad (1)$$

where  $J_{\mathbf{q}}$  and  $\mathbf{S}_{\mathbf{q}}$  are, respectively, Fourier transforms of

the exchange interaction and spin density

$$J_{\mathbf{q}} = N^{-1} \sum_{\mathbf{r}, \mathbf{r}'} J_{\mathbf{r}-\mathbf{r}'} \exp[i\mathbf{q} \cdot (\mathbf{r}-\mathbf{r}')], \quad (2)$$

$$\mathbf{S}_{\mathbf{q}} = N^{-1/2} \sum_{\mathbf{r}} \mathbf{S}_{\mathbf{r}} \exp(i\mathbf{q} \cdot \mathbf{r}). \quad (3)$$

Here we use the convention that  $J_{\mathbf{r}} < 0$  and  $J_{\mathbf{r}} > 0$  correspond to antiferromagnetic and ferromagnetic interactions, respectively. The minimum of  $\mathcal{H}$  occurs for the  $\mathbf{q}$  vector that maximizes  $J_{\mathbf{q}}$ . For general  $\mathbf{q}$ , a helical structure is stabilized.

As a prelude to understanding the rhombohedral lattice, we consider a model with an antiferromagnetic in-plane interaction  $J$  and interplanar interaction  $J' = 0$ . In this case (1) is minimized for in-plane wave vectors  $\pm(\frac{1}{3}, \frac{1}{3})$  (in the hexagonal metric), which corresponds to the  $120^\circ$  spin arrangement mentioned above. The wave vector along the  $z$  direction  $q_z$  does not affect the minimum in  $\mathcal{H}$ , since there is no interaction along this direction. Thus, one may express the ordering wave vectors as

$$\mathbf{q}_0 = \pm(\frac{1}{3}, \frac{1}{3}, q_z), \quad -\frac{\pi}{2} \leq q_z \leq \frac{\pi}{2}. \quad (4)$$

This is a trivial example of what Rastelli has called a *degeneration line*.<sup>6</sup> Since there are  $N^{1/3}$  possible values for  $q_z$  in (4), the ground-state degeneracy is proportional to  $N^{1/3}$ . The system is effectively two dimensional and, due to the famous theorem of Mermin and Wagner, one expects no long-range order at finite temperatures.<sup>7</sup> The presence of a degeneration line here is intuitively obvious, since  $J_{\mathbf{q}}$  is independent of  $q_z$  when  $J' = 0$ . Rastelli has shown that if  $J'$  is nonzero (either positive or negative, but  $|J'| < 3|J|$ ) the degeneration line persists but now maps out a nontrivial curved line in  $\mathbf{q}$  space.<sup>8</sup> For small  $j = J'/|J|$  the degeneration line is a spiral centered about the line defined in (4), which in real space translates into a

distortion of the  $120^\circ$  spin structure. Rastelli has calculated an expansion in  $j=J'/J$  for  $q_x$  and  $q_y$  in terms of  $q_z$  and plotted the degeneration lines for various values of  $j$ .<sup>8</sup>

The frustrated rhombohedral antiferromagnet as discussed above is realized in the  $\beta$  phase of solid oxygen<sup>9</sup> and also in  $\text{LiNiO}_2$  and  $\text{NaNiO}_2$  (Ref. 10) with spin quantum numbers of  $S=1$  for oxygen and  $S=\frac{1}{2}$  for  $\text{Ni}^{3+}$ . In both cases quantum fluctuations will be important and to a first approximation break the infinite ground-state degeneracy.<sup>11</sup> However, this quantum selection will only be effective at very low temperatures and hence is unimportant for our work at higher temperatures. Anderson has suggested that the spin- $\frac{1}{2}$  triangular lattice antiferromagnet is possibly a quantum spin liquid and cannot be described properly in the context of spin-wave theory.<sup>12</sup> The nature of the spin liquid phase is poorly understood and it is unclear whether or not spin-spin correlations in this phase will be strong enough to result in observed magnetic scattering. Neutron-scattering experiments on  $\beta$ -oxygen clearly show diffuse magnetic scattering that is attributed to short-range ordering of moments.<sup>9</sup> For

$\text{LiNiO}_2$  no such wide-angle magnetic scattering has been observed<sup>10</sup> but small-angle neutron-scattering experiments indicate that some ferromagnetic correlations set in at high temperature.<sup>13</sup>

Two other highly frustrated systems that are of current interest are the *kagomé* [Fig. 1(b)] and pyrochlore [Fig. 1(c)] lattices. The *kagomé* lattice can be pictured as a lattice of *corner-sharing* triangles and the pyrochlore lattice is made up of *corner-sharing* tetrahedra and is in some sense a three-dimensional analog of the *kagomé* lattice. In the absence of interactions beyond nearest-neighbor or anisotropy, these systems do not order at finite temperature.<sup>14,15</sup> Instead of having degeneration lines in  $q$  space, the two-dimensional *kagomé* antiferromagnet exhibits a degeneration *plane* in  $\mathbf{q}$  space<sup>16</sup> and the pyrochlore has a degeneration *volume*.<sup>16</sup> Neutron-diffraction studies on the stacked *kagomé* lattice material  $\text{SrCr}_{8-x}\text{Ga}_{4+x}\text{O}_{19}$  (Refs. 17 and 18) and a number of pyrochlore compounds [ $\text{Y}_2\text{Mn}_2\text{O}_7$  (Ref. 19),  $\text{Tb}_2\text{Mo}_2\text{O}_7$  (Refs. 20 and 21),  $\text{FeF}_3$  (Ref. 22), and  $\text{Mn}_2\text{Sb}_2\text{O}_7$  (Ref. 22)] exhibit diffuse neutron scattering over a wide range of temperatures and except for  $\text{FeF}_3$ , none has yet shown long-range magnetic order.

Here we calculate the diffuse magnetic scattering for these highly frustrated materials directly from the magnetic interaction models. Conventional Monte Carlo (MC) techniques and an analytic approach based on the Gaussian approximation (GA) are used. The motivation for this work is twofold: to understand some previous neutron-scattering studies, and to predict exchange constants based on modeling the observed diffuse scattering. Section II describes the Monte Carlo (MC) methods used and the neutron-scattering profile calculations. Section III develops the analytic approach that complements the MC method, and in Sec. IV the results for the two methods are discussed and compared. Comparisons are also made with experiment for some pyrochlore materials. Finally we summarize the important aspects of this work in Sec. V.

## II. MONTE CARLO METHODS

The simulations were carried out using the Metropolis spin-flipping algorithm. The number of spins considered ranged from  $N=100$  to 4800, and from  $N=128$  to 3456 for the 2D and 3D systems, respectively. Periodic boundary conditions were used to eliminate surface effects. Spin-spin correlation functions were averaged over 1000 configurations for the largest lattice sizes and over 100 000 configurations for the smallest lattice sizes, with 10 000 MC steps per spin discarded in order to reach equilibrium. The smaller number of averaged configurations for the larger lattice sizes results in no reduction in the quality of the results, since the number of bonds averaged increases like  $N$ . Successive spin configurations were separated by 10 MC steps per spin in an attempt to minimize autocorrelation effects. The random spin moves were attenuated by a factor  $\delta$ , which was adjusted in such a way that roughly 50% of attempted spin flips were accepted. This was very important for the low-temperature simulations. When a spin move was re-

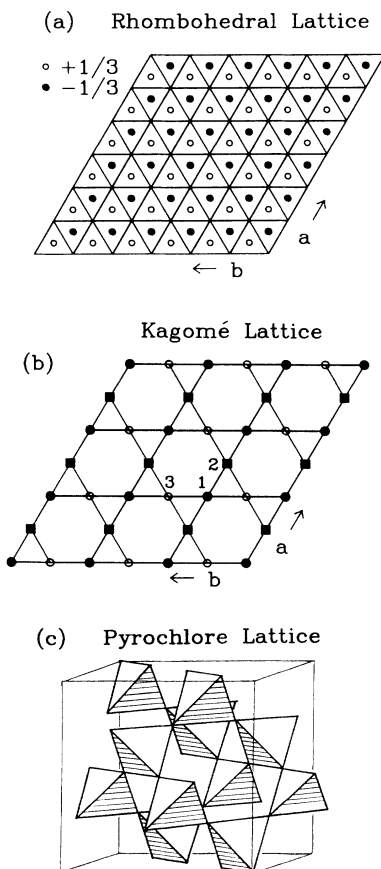


FIG. 1. Schematic diagrams of the three frustrated lattices studied. (a) The rhombohedral lattice with open and filled circles representing lattice sites above and below the plane of the page. The labels  $\frac{1}{3}$  and  $-\frac{1}{3}$  are fractional coordinates along the  $z$  direction. (b) The *kagomé* lattice with the three sublattices labeled. (c) The pyrochlore lattice, which is a three-dimensional network of corner sharing tetrahedra.

jected, the spin was then randomly pivoted around its local exchange field.<sup>23</sup> Such pivoting has no effect on the internal energy but increases the rate of phase-space sampling.

The simulations used a simple isotropic Heisenberg Hamiltonian

$$\mathcal{H} = -\frac{1}{2}J_{\text{NN}} \sum_{\langle ij \rangle_{\text{NN}}} \mathbf{S}_i \cdot \mathbf{S}_j - \frac{1}{2}J' \sum_{\langle ij \rangle} \mathbf{S}_i \cdot \mathbf{S}_j, \quad (5)$$

where  $\mathbf{S}_i = (S_i^x, S_i^y, S_i^z)$  is a classical unit spin at lattice site  $i$ .  $J_{\text{NN}}$  is the interaction between nearest neighbors and is negative or antiferromagnetic for all systems considered here.  $J'$  is the interplane interaction for the rhombohedral-lattice system and is not included in the pyrochlore- and *kagomé*- lattice models.

Here we calculate the powder-averaged neutron-scattering cross section, since the existing data for these materials was measured on polycrystalline samples. We find following Ref. 24 that

$$\frac{d\sigma}{d\Omega} = \frac{2}{3}(\frac{1}{2}\mu\gamma r_0)^2 [f(Q)]^2 \sum_{i,j} \langle \mathbf{S}_i \cdot \mathbf{S}_j \rangle \frac{\sin(QR_{ij})}{QR_{ij}}, \quad (6)$$

where  $(d\sigma/d\Omega)$  is the scattering cross section of neutrons per unit solid angle,  $\frac{1}{2}\gamma r_0 \approx 0.27 \times 10^{-12}$  cm, is the neutron-scattering length per Bohr magneton,  $\mu$  is the magnitude of the local spin moments,  $f(Q)$  is the magnetic form factor,  $Q$  is the magnitude of the neutron-scattering vector,  $\langle \mathbf{S}_i \cdot \mathbf{S}_j \rangle$  is the thermal expectation of the correlation between the spins at sites  $i$  and  $j$ , and  $R_{ij} = |\mathbf{R}_i - \mathbf{R}_j|$  is the distance between sites  $i$  and  $j$ . The factor of  $\frac{2}{3}$  arises because the neutrons only “see” the component of  $\mathbf{S}$  perpendicular to the scattering vector  $\mathbf{Q}$ . Thus for a system with isotropic interactions and no symmetry breaking long-range order, we have

$$\langle \mathbf{S}_i^{\perp} \cdot \mathbf{S}_j^{\perp} \rangle = \frac{2}{3} \langle \mathbf{S}_i \cdot \mathbf{S}_j \rangle. \quad (7)$$

For an  $L \times L \times L$  lattice with periodic boundary conditions, the maximum distance  $R_{ij}$  is  $\sqrt{3}(L/2)$  and for 2D lattices it is  $\sqrt{2}(L/2)$ . This is a shortcoming of the MC method for calculating the neutron-scattering profile. However, for the *kagomé* and pyrochlore systems the correlations die out rather quickly, and even at very low temperatures, lattice sizes that are manageable with MC are quite sufficient. For all but the smallest lattice sizes the double summation in (6) is the rate limiting step in the calculations. Therefore, we used an efficient histo-

$$\begin{aligned} \langle S_i^a \cdot S_j^b \rangle &= \frac{1}{N} \sum_{\mathbf{q}, \mathbf{q}'} \sum_{\alpha, \beta} \exp[-i\mathbf{q} \cdot (\mathbf{R}_i + \mathbf{r}_a)] \exp[-i\mathbf{q}' \cdot (\mathbf{R}_j + \mathbf{r}_b)] \Psi_{\mathbf{q}}^{\alpha a} \Psi_{\mathbf{q}'}^{\beta b} \langle \varphi_{\mathbf{q}}^{\alpha} \cdot \varphi_{\mathbf{q}'}^{\beta} \rangle \\ &= \frac{1}{N} \sum_{\mathbf{q}, \alpha} \exp[-i\mathbf{q} \cdot (\mathbf{R}_i - \mathbf{R}_j + \mathbf{r}_a - \mathbf{r}_b)] \Psi_{\mathbf{q}}^{\alpha a} \Psi_{-\mathbf{q}}^{\alpha b} [1 - \lambda_{\mathbf{q}}^{\alpha} / (3T)]^{-1}, \end{aligned} \quad (13)$$

where  $\mathbf{r}_a$  is the fractional coordinate of sublattice  $a$ . This can now be substituted into the neutron-scattering cross section similar to (6) that has not yet been powder averaged

$$\frac{d\sigma}{d\Omega} = \frac{2}{3}(\frac{1}{2}\mu\gamma r_0)^2 [f(Q)]^2 \sum_{i,j} \langle \mathbf{S}_i \cdot \mathbf{S}_j \rangle \exp(i\mathbf{Q} \cdot \mathbf{R}_{ij}), \quad (14)$$

gram method that reduces the number of  $\sin(QR)$  terms (by orders of magnitude) that must be evaluated.<sup>25</sup>

### III. THE GAUSSIAN APPROXIMATION (GA)

We start with a Landau expansion for the free energy in terms of Fourier modes

$$\mathcal{F}(T) = \frac{1}{2} \sum_{\mathbf{q}} \sum_{a,b} (nT\delta^{ab} - J_{\mathbf{q}}^{ab}) \langle \mathbf{S}_{\mathbf{q}}^a \rangle \cdot \langle \mathbf{S}_{-\mathbf{q}}^b \rangle + O(\langle S \rangle^4), \quad (8)$$

where we have introduced sublattice indexes  $a$  and  $b$ ,  $\delta^{ab}$  is a Kronecker delta and  $n=3$  is the number of spin components. The  $n$  arises from a mean-field theory derivation of (8).<sup>16</sup> The sublattice indices are necessary because the *kagomé* and pyrochlore lattices are not Bravais lattices, thus having more than one spin per unit cell and  $J_{\mathbf{q}}^{ab}$  is now a  $p \times p$  matrix,  $p$  being the number of sublattices. As a result, Fourier transforming is insufficient to diagonalize the second-order term in the Landau expansion. In diagonal form we have

$$\mathcal{F}(T) = \frac{1}{2} \sum_{\mathbf{q}, \alpha} (nT - \lambda_{\mathbf{q}}^{\alpha}) \varphi_{\mathbf{q}}^{\alpha} \cdot \varphi_{-\mathbf{q}}^{\alpha} + O(\varphi^4), \quad (9)$$

where the  $\lambda$ 's are eigenvalues of  $J_{\mathbf{q}}^{ab}$  and

$$\varphi_{\mathbf{q}}^{\alpha} = \sum_a \Psi_{\mathbf{q}}^{\alpha a} \langle \mathbf{S}_{\mathbf{q}}^a \rangle, \quad (10)$$

are linear combinations of Fourier modes that diagonalize  $J_{\mathbf{q}}^{ab}$ .  $\Psi_{\mathbf{q}}^{\alpha a}$  is the  $a$ th component of the  $\alpha$ th eigenvector of  $J_{\mathbf{q}}^{ab}$ .

In this language a phase transition to long-range order occurs at the mean-field critical temperature

$$T_c^{\text{MF}} = \frac{1}{n} \max_{\mathbf{q}, \alpha} \{\lambda_{\mathbf{q}}^{\alpha}\}, \quad (11)$$

where  $\max\{\}$  is a global maximum over all  $\mathbf{q}$  and  $\alpha$ . When  $T > T_c^{\text{MF}}$  one can apply the GA (neglect of  $\varphi^4$  and higher terms in the Landau expansion) and through functional integration (see Appendix A for details) obtain an estimate of the two-point correlation function<sup>26</sup>

$$\langle \varphi_{\mathbf{q}}^{\alpha} \cdot \varphi_{\mathbf{q}'}^{\beta} \rangle = 3\delta^{\alpha\beta} \delta(\mathbf{q} + \mathbf{q}') (3 - \lambda_{\mathbf{q}}^{\alpha} / T)^{-1}. \quad (12)$$

Back transforming to obtain the correlations in real space we have

where (7) has again been used. On substituting (13) and (14) one obtains the desired result

$$\begin{aligned} \frac{d\sigma}{d\Omega}(\mathbf{Q}) &= \frac{2}{3} N (\frac{1}{2}\mu\gamma r_0)^2 [f(Q)]^2 \\ &\times \sum_{\alpha} |F^{\alpha}(\mathbf{Q})|^2 [1 - \lambda_{\mathbf{Q}}^{\alpha} / (3T)]^{-1}, \end{aligned} \quad (15)$$

$$F^\alpha(\mathbf{Q}) = \sum_a \Psi_q^{aa} \exp(i\mathbf{r}_a \cdot \mathbf{Q}). \quad (16)$$

Where  $\mathbf{Q} = \mathbf{K} + \mathbf{q}$ ,  $\mathbf{K}$  is a reciprocal lattice vector and  $\mathbf{q}$  must lie within the first Brillouin zone. Due to the  $\mathbf{q}$  dependence of  $\lambda_q^\alpha$  and  $\Psi_q^{aa}$ , the powder average of (14) will, in general, be very complicated. An efficient numerical procedure for doing the powder average is outlined in Appendix B.

For large  $T$ , (14) reduces to the standard paramagnetic scattering cross section for a system with  $Np$  spins ( $N$  is

the number of unit cells and  $p$  is the number of sublattices)

$$\left[ \frac{d\sigma}{d\Omega} \right]_{\text{para}} = \frac{2}{3} Np \left( \frac{1}{2} \mu \gamma r_0 \right)^2 [f(Q)]^2. \quad (17)$$

Another limiting form arises when  $T$  is very close to but not less than  $T_c^{\text{MF}}$ . Here the scattering is dominated at  $\mathbf{q}$  vectors near the  $\mathbf{q}$  that maximizes  $\lambda_q^\alpha$ . If we expand  $\lambda_q^\alpha = \lambda_{\text{max}}^\alpha - e(\mathbf{q}_{\text{max}} - \mathbf{q})^2$ , we obtain

$$\frac{d\sigma}{d\Omega}(\mathbf{Q}) \propto \frac{2}{3} N \left( \frac{1}{2} \mu \gamma r_0 \right)^2 [f(Q)]^2 \sum_\alpha |F^\alpha(\mathbf{Q})|^2 [\xi^2 + (\mathbf{q}_{\text{max}} + \mathbf{K} - \mathbf{Q})^2]^{-1}, \quad (18)$$

$$\xi \propto \left[ \frac{T - T_c^{\text{MF}}}{T_c^{\text{MF}}} \right]^{1/2} = t^{1/2}, \quad (19)$$

which gives the standard Lorentzian form for peaks centered at satellites about reciprocal lattice vectors. Finally, in many neutron-scattering experiments a high-temperature data set is subtracted from a low-temperature one to remove nuclear Bragg peaks and isolate the diffuse magnetic scattering. Of course this also subtracts away the paramagnetic scattering. The difference profile is easily shown to be a minor modification of (15)

$$\left[ \frac{d\sigma}{d\Omega} \right]_{\text{diff}} = \frac{2}{3} N \left( \frac{1}{2} \mu \gamma r_0 \right)^2 [f(Q)]^2 \sum_\alpha |F^\alpha(\mathbf{Q})|^2 \frac{\lambda_q^\alpha}{3T - \lambda_q^\alpha}. \quad (20)$$

For most materials the isotropy assumption (7) is only approximately valid and a more general version of the cross section (15) for anisotropic systems is discussed in Appendix C.

## IV. RESULTS AND DISCUSSION

### A. Reduced units

We will attempt to compare the results from the two methods (MC and GA), and point out the advantages and disadvantages of each. To do this we assume that results for the same reduced temperature

$$t = (T - T_c) / T_c \quad (21)$$

are comparable. This is necessary as the transition temperature from mean-field theory,  $T_c^{\text{MF}}$ , is generally vastly different in highly frustrated systems, from the real  $T_c$ . For the 2D-triangular Heisenberg antiferromagnet, Kawamura and Miyashita<sup>27</sup> have shown that  $T_c \approx 0.33|J|$  and not zero as expected for a 2D system with vector spins.<sup>7</sup> They propose that the transition is most likely a Kosterlitz-Thoules transition associated with the pairing of chiral vortex pairs. For the *kagomé*- and pyrochlore-lattice systems the  $T_c$ 's are believed to be very low if not zero and here they are assumed to be zero. In this case scattering profiles calculated from the GA for

a given reduced temperature,  $t = (T - T_c^{\text{MF}}) / T_c^{\text{MF}}$  are compared with the same absolute temperature  $T/|J|$  from the MC simulations. However, as we shall see this did not prove to be very successful.

All results are plotted as a function of  $Q$  in both reciprocal lattice units (r.l.u.) and, where possible in terms of  $Q$  in  $\text{\AA}^{-1}$ , using a cell constant for the relevant material. This is convenient for comparison with previously obtained experimental data. Thus

$$Q(\text{\AA}^{-1}) = 2\pi \frac{Q(\text{r.l.u.})}{a_{\text{cell}}}, \quad (22)$$

and the cell constants used were  $a_{\text{cell}} = 6.0$  and  $10 \text{\AA}$  for  $\text{SrCr}_{8-x}\text{Ga}_{4+x}\text{O}_{19}$  (*kagomé* lattice) and  $\text{FeF}_3$ ,  $\text{Y}_2\text{Mn}_2\text{O}_7$ ,  $\text{Tb}_2\text{Mo}_2\text{O}_7$  (pyrochlore lattice), respectively. For the rhombohedral lattice the interplanar spacing affects the calculated scattering when  $J'$  is nonzero. For simplicity we have plotted the results for two cases; one in which the inter and intraplanar atomic distances are equal (ideal cubic close packed lattice) and secondly, for the interplanar spacing in  $\text{LiNiO}_2$ .

Scattering intensities are plotted in reduced units per spin so that the results are independent of the details of the magnetic form factor  $f(Q)$ , the size of the local moments and the system size

$$\left[ \frac{d\sigma}{d\Omega} \right]_{\text{red}} = \frac{d\sigma}{d\Omega} (Np)^{-1} [f(Q)]^{-2} \left( \frac{1}{2} \mu \gamma r_0 \right)^{-2}. \quad (23)$$

Any experimental neutron-scattering data can be compared with our results by simply scaling the data with the appropriate form-factor squared and an arbitrary multiplicative constant.

### B. The rhombohedral antiferromagnet

This Bravais lattice has one spin per rhombohedral unit cell (in the hexagonal system there would be three spins per unit cell) so we use Eq. (15) without eigenvalues and eigenvectors. Thus

$$\frac{d\sigma}{d\Omega}(\mathbf{Q}) = \frac{2}{3} N \left( \frac{1}{2} \mu \gamma r_0 \right)^2 [f(Q)]^2 [1 - J_q / (3T)]^{-1} \quad (24)$$

and using (2)

$$J_q = 2J[\cos(2q_x - 2q_y) + \cos(2q_y - 2q_z) + \cos(2q_z - 2q_x)] \\ + 2J'[\cos(2q_x) + \cos(2q_y) + \cos(2q_z)]. \quad (25)$$

The GA and MC results for case  $J'=0$  are shown in Fig. 2. The expected two-dimensional peak shapes arising from rods of scattering along the  $q_z$  direction are observed. The three peaks correspond to rods at

$$\mathbf{q} = (\frac{1}{3}, \frac{1}{3}, q_z)_H, (\frac{2}{3}, \frac{2}{3}, q_z)_H, (\frac{1}{3}, \frac{4}{3}, q_z)_H,$$

where the subscript  $H$  refers to the hexagonal metric that experimentalists use. For ideal long-range order in the basal planes, the peaks should have no tail on the low- $Q$  side. A tail is observed, since  $T > T_c$  and any correlations are finite in extent. Spurious oscillations in the MC data are due to the sharp cutoff of (6) due to the finite size of the simulations. The MC scattering is also always weaker than that obtained from the GA, since the neglected fourth-order term [which is positive definite in (8)] is neglected in the GA (but not in MC) and tends to concentrate the weights in the partition function more towards small spin expectation values.

Figure 3 shows scattering profiles for seven different values of  $j = J'/|J|$  as calculated from (24) for three temperatures with an ideal close-packed interplanar spacing. The MC methods were not effective here; extremely large lattices with  $N \approx 50000$  spins would be required to see reasonably sharp peaks. One effect of the interplanar interaction is the shift in the low angle peak position as a function of  $J'$ . The peaks are seen to remain quasi-two-dimensional in shape for  $|j| \leq 1$ . At high temperature the peaks become more symmetric about the center, which could be a possible explanation for the experimental results in  $\beta$ -oxygen.<sup>9,28</sup> The small-angle neutron scattering (SANS) increases rapidly at low  $Q$ , as  $J'$  becomes large and positive. The model with  $J' = -1$  corresponds to the fcc antiferromagnet. Figure 4 shows the scattering for the same interactions used in Fig. 3 but using the interplanar spacing of  $\text{LiNiO}_2$ . In order to interpret these results we will present below a discussion of scattering from helical degeneration lines.

As stated previously, Rastelli and Tassi<sup>11</sup> have calcu-

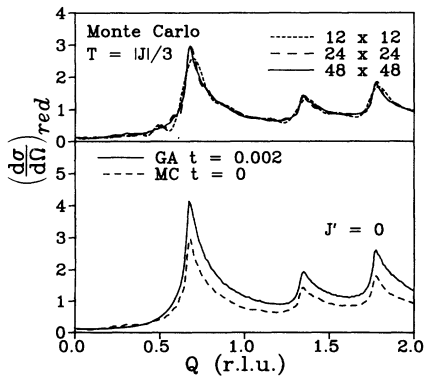


FIG. 2. Top: MC results of the rhombohedral antiferromagnet near  $T_c$  with no interplanar interaction. Bottom: Comparison of the MC ( $L = 48 \times 48$ ) and GA profiles.

lated an expansion for the degeneration line of rhombohedral antiferromagnets with interplanar interactions. To first order in  $j = J'/|J|$  the line is a helix centered at  $\mathbf{q}_0 = (\frac{1}{3}, \frac{1}{3}, q_z)$  with radius  $\delta = 2j/(\sqrt{3}a)$ . In an orthogonal coordinate system we parameterize the helix in terms of  $\tau$  giving

$$Q_x = q_0 - \delta \cos(\tau), \quad (26a)$$

$$Q_y = \delta \sin(\tau), \quad (26b)$$

$$Q_z = 3\tau/c, \quad (26c)$$

and

$$Q = [\delta^2 - 2\delta q_0 \cos(\tau) + q_0^2 + 9\tau^2/c^2]^{1/2}. \quad (27)$$

The pitch of the helix is determined by the interplanar spacing, i.e., by the ratio  $a/c$ . Scattering will only occur if  $Q$  makes contact with the degeneration helix. The scattered intensity is proportional to the density of states  $\rho(Q)$  at the point of contact. For a helix there will often be numerous points of contact for a given  $|Q|$  due to the periodicity of the  $\cos(t)$  term in (27). Figure 5(a) shows schematically the degeneration helix intersecting spheres

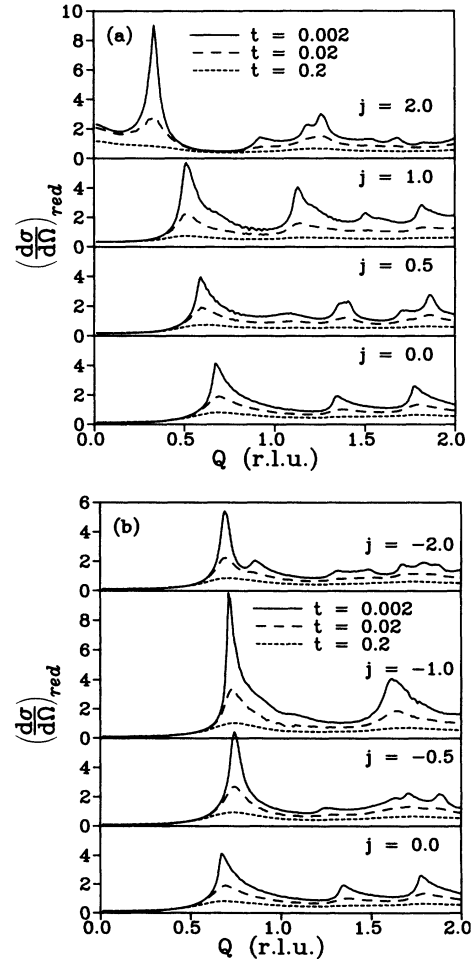


FIG. 3. GA profiles for various temperatures and values of the interplanar interaction  $j = J'/|J|$ . The interplanar spacing corresponds to that of an ideal cubic close-packed structure.

in  $\mathbf{q}$  space. The sphere of radius  $Q_1$  corresponds to the first 2D peak at  $Q=q_0-\delta$ . As  $J'$  becomes larger so does  $\delta$  and the peak moves to lower  $Q$  as observed in Figs. 3(a) and 4(a) for  $j>0$ . Further peaks at higher  $Q$  will also arise from other nodes in the helix as exemplified by  $Q_2$  and  $Q_3$  in Fig. 5(a).

With these ideas in mind we can calculate a zero-temperature cross section. Assuming the density of states is constant in  $\tau$

$$\begin{aligned} \rho(\tau) &= \text{const} \\ &= \left| \frac{dN}{d\tau} \right| = \left| \frac{dN}{dQ} \frac{dQ}{d\tau} \right| = \rho(Q) \left| \frac{dQ}{d\tau} \right|. \end{aligned} \quad (28)$$

Thus

$$\frac{d\sigma}{d\Omega_Q} \propto \rho(Q) \propto \left| \frac{d\tau}{dQ} \right|, \quad (29)$$

and using (27) we obtain the desired result

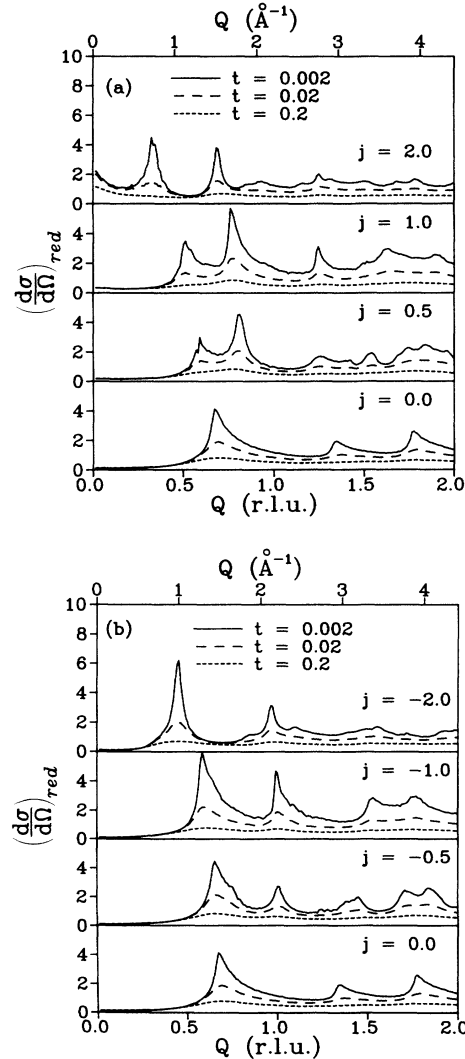


FIG. 4. As in Fig. 3, except with the interplanar spacing of  $\text{LiNiO}_2$ .

$$\frac{d\sigma}{d\Omega_Q} \propto \frac{Q(\tau)}{|9\tau/c^2 + \delta q_0 \sin(\tau)|}. \quad (30)$$

Setting the helix radius to  $\delta=0$  we then recover the standard cross section originally derived by Warren<sup>29</sup> for scattering from a rod in reciprocal space.

$$\frac{d\sigma}{d\Omega_Q} \propto \frac{Q}{(Q^2 - q_0^2)^{1/2}}. \quad (31)$$

Sharp 2D-diffraction peaks will occur at singularities in (30) with the peak positions depending on  $j$  and  $a/c$  in a nontransparent manner. Figure 5(b) shows the cross section calculated from (30) using the same parameters ( $\delta, q_0$ ) as in Fig. 5(a). The peak at  $Q_3$  is seen to have its tail on the low- $Q$  side instead of the high- $Q$  side. These inverted 2D peaks will occur whenever  $Q$  makes contact with a node on the back side of the helix. As far as we know such inverse Warren peaks are unique to systems with helical degeneration lines.

Now we are in a position to understand the existence

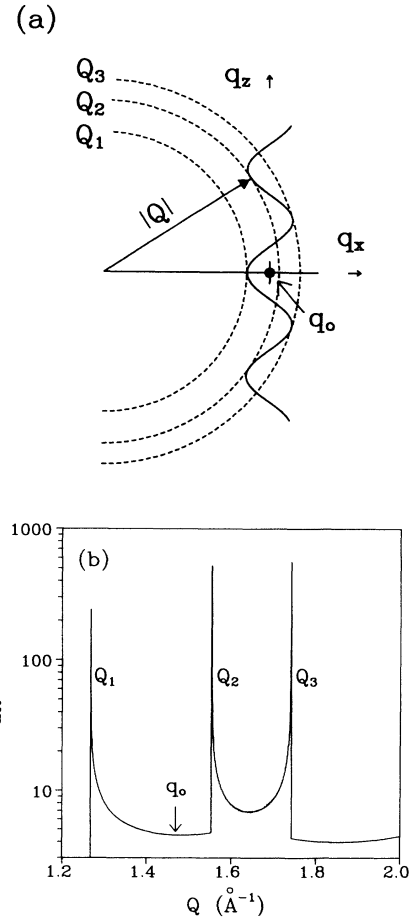


FIG. 5. (a) Schematic view of the various ways the scattering vector  $Q$  can make contact with a degeneration helix. When  $Q$  contacts the front of the helix as in the case of  $Q_1$  and  $Q_2$  a normal 2D Warren peak shape occurs in the scattering pattern and for  $Q_3$ , which contacts the back of the helix an inverted Warren peak shape occurs. (b) The diffraction pattern calculated from (30) using the same  $q_0$  and  $\delta$  used in (a).

and shape of the second peak in Fig. 4(a) for  $j=0.5$ . It arises from higher order nodes (one at the front and one at the back) of the degeneration helix centered at  $(\frac{1}{3}, \frac{1}{3}, q_z)_H$ . The peak is symmetric because there are actually two peaks back to back, one normal and one inverted. A similar situation arises in Fig. 4(b) for  $j=-0.5$ . An understanding of the patterns for  $|j| \geq 1$  is not so transparent, since the helical approximation (26) is no longer valid.<sup>8,11</sup>

### C. Kagome and pyrochlore antiferromagnets

For these systems one must keep in mind that there are three and 16 spins per unit cell for the *kagome* and pyrochlore lattices, respectively. Thus we have  $N=3L^2$  for the *kagome* lattice and  $N=16L^3$  for the pyrochlore lattice. The MC results for three *kagome*-lattice sizes ( $N=300$ , 1200, and 4800) at a low temperature are shown in Fig. 6(a) with no noticeable finite-size effects. The lack of sharp features points clearly towards short-range order. Recent theoretical work on the *kagome* antiferromagnet has shown that nematic order is possible in this system.<sup>30</sup> Long-range nematic order is however not observable with neutrons. Other work based on a high-temperature series expansion for classical spins proves that the  $q$ -space degeneracy, present at the mean-field level of approximation, is broken by thermal fluctua-

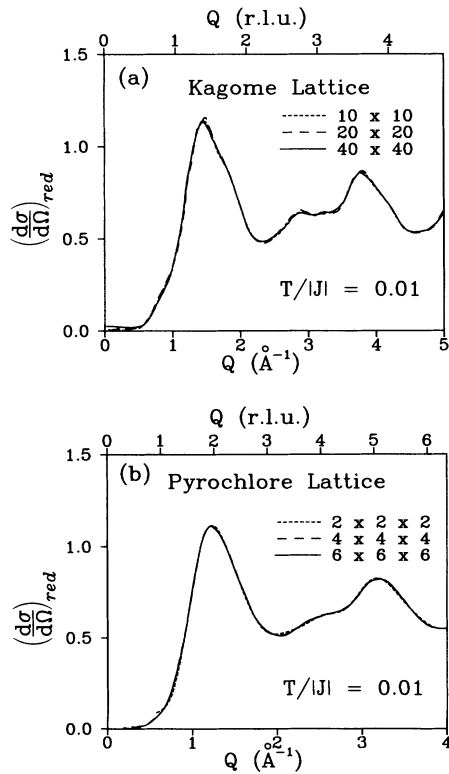


FIG. 6. MC profiles of the *kagome* (a) and pyrochlore (b) antiferromagnets for various lattice sizes at low temperature. Virtually no lattice size dependence is evident, indicating that correlations are truly short range.

tions.<sup>31</sup> At eighth order in  $J/T$  the system selects a  $\sqrt{3} \times \sqrt{3}$  structure for *XY* and Heisenberg spins. It is not clear how strong the thermal selection is and for a two-dimensional system, as studied here, the ordered phase will only be stable at  $T=0$ .

The MC results [Fig. 6(b)] for three pyrochlore-lattice sizes ( $N=128$ , 1024, and 3456, corresponding to  $L=2$ , 4, and 6, respectively) also exhibit virtually no size dependence between the two largest lattice sizes. This clearly shows that correlations do not extend beyond two unit cell lengths at this low temperature. We have shown that neither of these systems exhibits conventional long-range order down to rather low temperatures on the order of  $T/|J|=0.01$ . In fact, the ground states of both systems are infinitely degenerate making thermal selection of a long-range-ordered state at low temperatures difficult.

In Fig. 7, a comparison of the MC and GA results are shown for various temperatures. At low temperatures the agreement is reasonable and as usual the GA results overestimate the intensity of the scattering. However at the higher temperatures the opposite is true. Assuming  $T_c=0$  for these systems and recalling that  $T_c^{Mf} \neq 0$ , a direct comparison of either absolute or reduced temperatures between the MC and GA is not possible. This is not a serious problem, since one must rescale all results by an arbitrary multiplicative constant in order to compare with experiment.

Figure 8 shows a comparison of the MC and GA

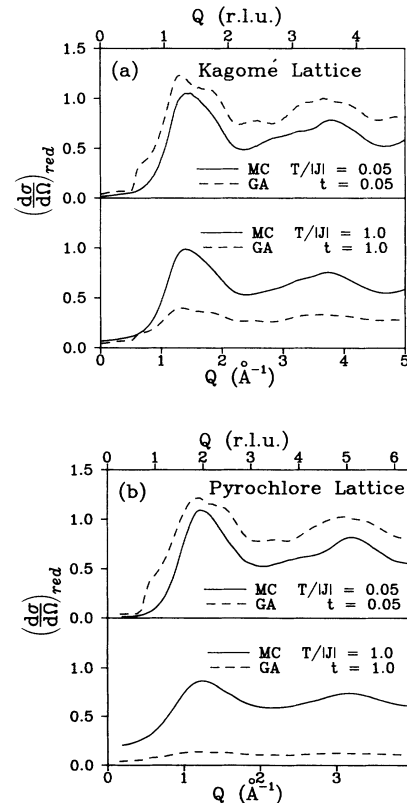


FIG. 7. Comparison of the MC and GA results for the *kagome* (a) and pyrochlore (b) antiferromagnets.

profiles with previously reported neutron-diffraction data for  $\text{FeF}_3$  (Ref. 22) and  $\text{Tb}_2\text{Mo}_2\text{O}_7$  (Ref. 20). In both cases a high-temperature data set has been subtracted in order to isolate the magnetic scattering. Due to changes with temperature of the Debye-Waller factor, some sharp features remain at nuclear Bragg angles. For  $\text{FeF}_3$  the agreement is rather satisfactory except at low  $Q$ , where the GA overestimates the intensity. The agreement for  $\text{Tb}_2\text{Mo}_2\text{O}_7$  with the MC profile is also good, however the GA was not as successful. The GA was indispensable as a tool for rapidly finding approximate exchange constants. This model is significantly more complicated as both  $\text{Tb}^{3+}$  ( $\mu \approx 9\mu_B$ ) and  $\text{Mo}^{4+}$  ( $\mu \approx 1\mu_B$ ) are magnetic. Thus we must now choose three exchange constants  $J_{\text{Mo-Mo}}$ ,  $J_{\text{Tb-Mo}}$ , and  $J_{\text{Tb-Tb}}$  in order to model the data. Reasonable results were obtained by a trial and error choice of  $J_{\text{Mo-Mo}}=0$ ,  $J_{\text{Tb-Mo}}=1.0$ , and  $J_{\text{Tb-Tb}}=-0.01$ . The results were very sensitive to the value of  $J_{\text{Tb-Tb}}$  due to the large  $\text{Tb}^{3+}$  magnetic moment. Similarly, small values for  $J_{\text{Mo-Mo}}$  had little effect because of the small  $\text{Mo}^{4+}$  moment. Better results may be obtained with a considerably more complicated calculation (Appendix C) that includes the anisotropy for  $\text{Tb}^{3+}$ .

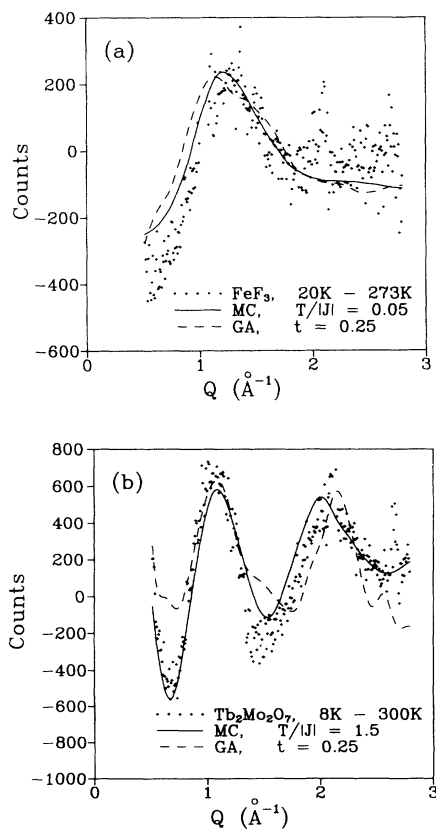


FIG. 8. Comparison of MC, GA, and experimental diffuse magnetic scattering profiles for two pyrochlore compounds  $\text{FeF}_3$  (a) and  $\text{Tb}_2\text{Mo}_2\text{O}_7$  (b). High-temperature data sets have been subtracted in order to isolate the magnetic scattering. Residual nuclear Bragg peaks are still evident in the subtraction at  $Q=2.0$  and  $2.6 \text{ \AA}^{-1}$  for  $\text{FeF}_3$  and  $Q=2.6 \text{ \AA}^{-1}$  for  $\text{Tb}_2\text{Mo}_2\text{O}_7$ .

## V. CONCLUSIONS

A straightforward method for calculating diffuse magnetic scattering profiles directly from exchange constants has been presented. Analytic expressions were derived for a number of cases, isotropic exchange, anisotropic exchange, and difference scattering, all for general non-Bravais lattices. The results agree well with MC calculations to within an overall scale factor. The MC and GA methods are complimentary, since MC takes account of thermal fluctuations exactly but is inefficient for systems with long-range correlations. Conversely, the GA method does not suffer from finite-size effects but only takes thermal fluctuations into account in an approximate manner. As well the GA calculations were more rapid allowing trial and error fitting of experimental data by adjusting the interactions. In principle a least-squares fitting approach is possible where temperature, scale factor, exchange constants, and possibly even anisotropies are taken as refinable parameters.

The GA results for the rhombohedral-lattice antiferromagnet aid in the interpretation of experimental results for  $\text{LiNiO}_2$ . Previous searches for magnetic scattering in  $\text{LiNiO}_2$  focused near the  $(\frac{1}{3}, \frac{1}{3}, q_z)$  Bragg angles.<sup>10</sup> Our results (Fig. 4) showed that a ferromagnetic interplanar interaction shifts the  $(\frac{1}{3}, \frac{1}{3}, q_z)$  peak to lower  $Q$  where it may have been overlooked by the experiment.<sup>10</sup> Recent SANS experiments have shown that ferromagnetic correlations are present in  $\text{LiNiO}_2$  below 220 K.<sup>13</sup> The calculations also indicate that the pseudo-two-dimensional peaks become more symmetric about their centers as temperature is raised. This may explain the seemingly symmetric diffuse scattering profile observed in  $\beta$ -oxygen.<sup>9,28</sup> An understanding of the complicated diffraction profiles for rhombohedral antiferromagnets is facilitated by direct calculations of the cross section from a helical line of scattering in  $\mathbf{q}$  space. The helical model also predicts inverted 2D peaks with the tail on the low- $Q$  side, which are unique to such helical model systems.

For the *kagomé* and pyrochlore lattices, the MC method was more effective, since the correlations in these systems are short ranged at all finite temperatures. Satisfactory agreement with experiment was obtained for both the GA and MC methods with MC giving noticeably better results. The GA was used to find suitable exchange constants by trial and error, to model the neutron-diffraction data for  $\text{Tb}_2\text{Mo}_2\text{O}_7$ . Modeling this diffuse scattering with a standard Lorentzian line shape centered at an assumed ordering wave vector is seen to be incorrect, since there really is no ordering wave vector for the *kagomé*- and pyrochlore-lattice antiferromagnets.

These ideas should be applicable to other nonspin systems such as short-range-ordered lattice gases and binary alloy systems with frustrated interactions that inhibit long-range order over wide temperature ranges.

## ACKNOWLEDGMENTS

I would like to thank J. R. Dahn for a critical reading of this manuscript, useful discussions, and for providing access to the computer facilities used in the calculations.

Partial financial assistance from the Natural Sciences and Engineering Research Council of Canada is also acknowledged.

#### APPENDIX A: GAUSSIAN INTEGRATION

In order to prove (11) we start with the free energy to second order in the field variables with the summation over vector components  $\varphi = (\varphi^x, \varphi^y, \varphi^z)$  made explicit

$$\mathcal{F} = \frac{1}{2} \sum_{\mathbf{q}, \alpha, \varepsilon} (3T - \lambda_{\mathbf{q}}^{\alpha}) |\varphi_{\mathbf{q}}^{\alpha, \varepsilon}|^2 - T \sum_{\mathbf{q}, \alpha, \varepsilon} h_{\mathbf{q}}^{\alpha, \varepsilon} \varphi_{\mathbf{q}}^{\alpha, \varepsilon}. \quad (\text{A1})$$

Where  $\varepsilon = (x, y, z)$  and a local-field or source term,  $h$  has been added. Since (A1) is diagonal in the fields, the partition function factors

$$Z = \int \{d\varphi\} \exp(-\mathcal{F}/T) = \prod_{\mathbf{q}, \alpha, \varepsilon} Z_{\mathbf{q}}^{\alpha, \varepsilon}, \quad (\text{A2})$$

where

$$\int \{d\varphi\} = \prod_{\mathbf{q}, \alpha, \varepsilon} \left\{ \int d\varphi_{\mathbf{q}}^{\alpha, \varepsilon} \right\} \quad (\text{A3})$$

and

$$Z_{\mathbf{q}}^{\alpha, \varepsilon} = \int_{-\infty}^{\infty} d\varphi_{\mathbf{q}}^{\alpha, \varepsilon} \exp\left[-\frac{1}{2}(3 - \lambda_{\mathbf{q}}^{\alpha}/T) |\varphi_{\mathbf{q}}^{\alpha, \varepsilon}|^2 + h_{\mathbf{q}}^{\alpha, \varepsilon} \varphi_{\mathbf{q}}^{\alpha, \varepsilon}\right]. \quad (\text{A4})$$

From (A2) and (A4) one can see that

$$\langle \varphi_{\mathbf{q}}^{\alpha, \varepsilon} \varphi_{\mathbf{q}}^{\beta, \gamma} \rangle = Z^{-1} \int \{d\varphi\} \varphi_{\mathbf{q}}^{\alpha, \varepsilon} \varphi_{\mathbf{q}}^{\beta, \gamma} \exp(-\mathcal{F}/T) \quad (\text{A5})$$

$$= Z^{-1} \left. \frac{\partial^2 Z}{\partial h_{\mathbf{q}}^{\alpha, \varepsilon} \partial h_{\mathbf{q}}^{\beta, \gamma}} \right|_{h=0}. \quad (\text{A6})$$

Applying the standard identity

$$\int_{-\infty}^{\infty} dx \exp(-\frac{1}{2}Ax^2 + Bx) = \left[ \frac{2\pi}{A} \right]^{1/2} \exp\left[ \frac{|B|^2}{2A} \right], \quad A > 0, \quad (\text{A7})$$

to (A4) and substituting into (A3) we have

$$Z = \exp\left[ \frac{1}{2} \sum_{\mathbf{q}, \alpha, \varepsilon} \frac{|h_{\mathbf{q}}^{\alpha, \varepsilon}|^2}{3 - \lambda_{\mathbf{q}}^{\alpha}/T} \right] \prod_{\mathbf{q}, \alpha} \left[ \frac{2\pi}{3 - \lambda_{\mathbf{q}}^{\alpha}/T} \right]^{3/2}, \quad (\text{A8})$$

where the product over spin components ( $\varepsilon$ ) has been carried out. Finally substituting (A8) into (A6) we have the desired result

$$\langle S_i^{a,r} S_j^{b,s} \rangle = \frac{1}{N} \sum_{\mathbf{q}, \alpha, \rho} \sum_{\rho} \exp[-i\mathbf{q} \cdot (\mathbf{R}_i - \mathbf{R}_j + \mathbf{r}_a - \mathbf{r}_b)] \Psi_{\mathbf{q}}^{a\rho} \Psi_{\mathbf{q}}^{b\rho} (3 - \lambda_{\mathbf{q}}^{\alpha, \rho}/T)^{-1}, \quad (\text{C3})$$

where  $\alpha$  and  $\rho$  label the normal modes. (C3) must now be substituted into the general expression for elastic magnetic neutron scattering

$$\frac{d\sigma}{d\Omega} = (\frac{1}{2}\gamma r_0)^2 \sum_{i,j} \sum_{r,s} \langle S_i^r S_j^s \rangle f_i f_j \mu_i \mu_j \left[ \delta^{rs} - \frac{Q^r Q^s}{Q^2} \right] \exp(i\mathbf{Q} \cdot \mathbf{R}_{ij}) \quad (\text{C4})$$

$$\langle \varphi_{\mathbf{q}}^{\alpha} \cdot \varphi_{\mathbf{q}'}^{\beta} \rangle = 3\delta^{\alpha\beta} \delta(\mathbf{q} + \mathbf{q}') (3 - \lambda_{\mathbf{q}}^{\alpha}/T)^{-1}. \quad (\text{A9})$$

The restriction that  $A > 0$  in (A7) translates, in our context, into  $T > T_c^{\text{MF}}$ .

#### APPENDIX B: POWDER AVERAGING

The powder average of (14) is most easily carried out by first calculating all eigenvalues and eigenvectors over a grid in the first zone. As these are used repeatedly, once for each reciprocal lattice point considered, the results are saved on disk along with  $\lambda_{\text{max}}$ . If sharp features are present a grid size on the order of  $20 \times 20 \times 20$  or larger is necessary to minimize noise in the final profile. Next, a list of reciprocal lattice points ( $hkl$ ) that are within the desired  $Q$  range is calculated. Thus, a general point in reciprocal space can be expressed as

$$\mathbf{Q} = \mathbf{K} + \mathbf{q} = (h, k, l) + (q_x, q_y, q_z), \quad (\text{B1})$$

and  $\mathbf{q}$  lies in the first zone. The program now loops through  $\mathbf{Q}$  space with the loops over  $\mathbf{q}$  outside the loops over  $\mathbf{K}$ . If  $|\mathbf{Q}|$  is in range, then  $(d\sigma/d\Omega)(\mathbf{Q})$  is calculated from (14) and (15). The results are binned in a cross-section histogram. A second histogram containing the number hits in each bin of the cross section histogram is also maintained. This is used for normalizing the results at the end of the calculation. For profiles shown in this work at least  $10^7$   $\mathbf{Q}$ -space points were included in the calculations.

#### APPENDIX C: ANISOTROPIC SYSTEMS

Dealing with anisotropic Hamiltonians such as

$$H = -\frac{1}{2} \sum_{r,r'} \sum_{a,b} \sum_{r,s} J_{r-r'}^{ab,rs} S_r^{a,r} S_r^{b,s} \quad (\text{C1})$$

is straightforward and merely involves some extra baggage in the notation. Here we have written the summation over spin components  $s, r = (x, y, z)$  explicitly and  $J^{ab,rs}$  now depends on the direction in spin space. As before we can obtain the correlations in terms of eigenvalues and eigenvectors of  $J_{\mathbf{q}}^{ab,rs}$ , which is now a  $3p \times 3p$  matrix. Thus

$$\langle \varphi_{\mathbf{q}}^{\alpha, \rho} \varphi_{\mathbf{q}'}^{\beta, \sigma} \rangle = \delta^{\rho\sigma} \delta^{\alpha\beta} \delta(\mathbf{q} + \mathbf{q}') (3 - \lambda_{\mathbf{q}}^{\alpha, \rho}/T)^{-1}, \quad (\text{C2})$$

and

giving

$$\frac{d\sigma}{d\Omega}(\mathbf{Q}) = N(\frac{1}{2}\gamma r_0)^2 \sum_{\alpha,\rho} |\mathbf{F}_1^{\alpha,\rho}(\mathbf{Q})|^2 (3 - \lambda_{\mathbf{q}}^{\alpha,\rho}/T)^{-1}, \quad (\text{C5})$$

where

$$\mathbf{F}^{\alpha,\rho}(\mathbf{Q}) = \sum_a \mu_a f_a(Q) \Psi_{\mathbf{q}}^{\alpha,\rho} \exp(i\mathbf{r}_a \cdot \mathbf{Q}) \quad (\text{C6})$$

and

$$\mathbf{F}_1 = \mathbf{F} - (\mathbf{F} \cdot \hat{\mathbf{Q}}) \hat{\mathbf{Q}}. \quad (\text{C7})$$

Here we have also generalized the expression to include systems for which the moments and form factors on each sublattice are different. This was necessary for the  $\text{Tb}_2\text{Mo}_2\text{O}_7$  calculation.

- 
- <sup>1</sup>G. H. Wannier, *Phys. Rev.* **79**, 357 (1950).  
<sup>2</sup>A. Dannieian, *Phys. Rev.* **133**, A1344 (1964).  
<sup>3</sup>J. M. Coey, *Can. J. Phys.* **65**, 1210 (1987).  
<sup>4</sup>H. Kawamura, *J. Phys. Soc. Jpn.* **58**, 584 (1989); T. E. Mason, B. D. Gaulin, and M. F. Collins, *Phys. Rev. B* **39**, 586 (1989); H. Kadowaki, K. Ubokoski, K. Hirakawa, J. L. Martinez, and G. Shirane, *J. Phys. Soc. Jpn.* **56**, 1294 (1987).  
<sup>5</sup>K. Binder and A. P. Young, *Rev. Mod. Phys.* **58**, 801 (1986).  
<sup>6</sup>E. Rastelli, L. Reatto, and A. Tassi, *J. Phys. C* **16**, L331 (1983).  
<sup>7</sup>N. D. Mermin and H. Wagner, *Phys. Rev. Lett.* **17**, 1133 (1966).  
<sup>8</sup>E. Rastelli and A. Tassi, *J. Phys. C* **19**, L423 (1986); **20**, L303 (1987).  
<sup>9</sup>M. F. Collins, *Proc. Phys. Soc. London* **89**, 415 (1966); P. W. Stephens, R. J. Birgeneau, C. F. Majkrzak, and G. Shirane, *Phys. Rev. B* **28**, 452 (1983); R. J. Meier and R. B. Helmholdt, *ibid.* **29**, 1387 (1984).  
<sup>10</sup>K. Hirakawa, H. Kadowaki, and K. Ubukoshi, *J. Phys. Soc. Jpn.* **54**, 3526 (1985).  
<sup>11</sup>E. Rastelli and A. Tassi, *J. Phys. C* **21**, L35 (1988).  
<sup>12</sup>P. W. Anderson, *Mater. Res. Bull.* **8**, 153 (1973); P. Fazekas and P. W. Anderson, *Philos. Mag.* **30**, 423 (1974).  
<sup>13</sup>H. Yoshizawa, H. Mori, K. Hirota, and M. Ishikawa, *J. Phys. Soc. Jpn.* **59**, 2631 (1990).  
<sup>14</sup>V. Elser, *Phys. Rev. Lett.* **52**, 2405 (1989); I. Ritchey, P. Colmen, and P. Chandra (unpublished).  
<sup>15</sup>J. N. Reimers, *Phys. Rev. B* **45**, 7287 (1992).  
<sup>16</sup>J. N. Reimers, A. J. Berlinsky, and A.-C. Shi, *Phys. Rev. B* **43**, 865 (1991).  
<sup>17</sup>C. Broholm, G. Aeppli, G. P. Espinosa, and A. S. Cooper, *Phys. Rev. Lett.* **65**, 3173 (1990).  
<sup>18</sup>A. P. Ramirez, G. P. Espinosa, and A. S. Cooper, *Phys. Rev. Lett.* **64**, 2070, (1990).  
<sup>19</sup>J. N. Reimers, J. E. Greedan, R. K. Kremer, E. Gmelin, and M. A. Subramanian, *Phys. Rev. B* **43**, 3387 (1991).  
<sup>20</sup>J. E. Greedan, J. N. Reimers, C. V. Stager, and S. L. Penny, *Phys. Rev. B* **43**, 5682 (1991).  
<sup>21</sup>B. D. Gaulin, J. N. Reimers, J. E. Greedan, T. E. Mason, and Z. Tun (unpublished).  
<sup>22</sup>J. N. Reimers, J. E. Greedan, C. V. Stager, and M. Bjorgvinnsen, *Phys. Rev. B* **43**, 5692 (1991).  
<sup>23</sup>J. F. Fernandez and T. S. Streit, *Phys. Rev. B* **25**, 6910 (1982).  
<sup>24</sup>E. F. Bertaut and P. Burlet, *Solid State Commun.* **5**, 279 (1967).  
<sup>25</sup>B. D. Hall and R. Monot, *Comput. Phys.* **5**, 414 (1991).  
<sup>26</sup>See, for example, K. G. Wilson and J. B. Kogut, *Phys. Rep.* **12c**, 77 (1974); D. J. Amit, *Field Theory, the Renormalization Group, and Critical Phenomena* (World Scientific, Singapore, 1984); L. H. Ryder, *Quantum Field Theory* (Cambridge University Press, Cambridge, England, 1985); J. Zinn-Justin, *Quantum Field Theory and Critical Phenomena* (Oxford University Press, Oxford, 1990).  
<sup>27</sup>H. Kawamura and Miyashita, *J. Phys. Soc. Jpn.* **53**, 4138 (1984).  
<sup>28</sup>E. Rastelli, L. Reatto, and A. Tassi, *J. Phys. C* **19**, L589 (1986).  
<sup>29</sup>B. E. Warren, *Phys. Rev. B* **59**, 693 (1941).  
<sup>30</sup>J. T. Chalker, P. C. W. Holdsworth, and E. F. Shender (unpublished).  
<sup>31</sup>A. B. Harris, C. Kallin, and A. J. Berlinsky, *Phys. Rev. B* **45**, 2899 (1992).